

# Neutrino Observations of LHAASO Sources: Present and Prospect

Tian-Qi Huang,<sup>1,2</sup>★ and Zhuo Li,<sup>1,2</sup>†

<sup>1</sup>Department of Astronomy, School of Physics, Peking University, Beijing 100871, People’s Republic of China

<sup>2</sup>Kavli Institute for Astronomy and Astrophysics, Peking University, Beijing 100871, People’s Republic of China

Accepted XXX. Received YYY; in original form ZZZ

## ABSTRACT

The Large High Altitude Air Shower Observatory (LHAASO) observed a dozen of gamma-ray sources with significant emission above 100 TeV, which are the possible accelerators of PeV cosmic-rays. The neutrino observations are required to answer whether these high energy gamma-rays are generated through hadronic process (by cosmic-rays) or leptonic process (by electrons). We use the Bayesian method and the ten-year (2008–2018) IceCube data to constrain the hadronic gamma-ray flux from LHAASO sources. The current observations constrain that the hadronic component contributes no more than  $\sim 70\%$  to the gamma-rays from Crab Nebula, which disfavors the hadronic origin of gamma-rays below hundreds of TeV. For other LHAASO sources, the 90% C.L. upper limits on hadronic gamma-ray flux are still higher than the gamma-ray flux observed. The uncertainties due to the source extension assumption and statistical approach are discussed quantitatively. We also evaluate the neutrino observation of LHAASO sources in the combined search using the current and future neutrino telescopes.

**Key words:** neutrinos – gamma-rays:general – cosmic rays – methods: statistical

## 1 INTRODUCTION

The origins of high energy cosmic-rays are still unclear. Their trajectories are deflected from the direction of accelerator by the astrophysical magnetic field. Fortunately, these cosmic-rays could interact with baryon background or radiation field around the accelerators and generate high energy gamma-rays (via  $\pi^0$  decay) and neutrinos (via  $\pi^\pm$  decay), which are good indicators of cosmic-ray sources.

The most energetic photon ever observed is 1.4 PeV from the direction of Cygnus OB2, which was detected by the km<sup>2</sup> array (KM2A) of the Large High Altitude Air Shower Observatory (LHAASO) (Cao et al. 2021a). LHAASO-KM2A also observed significant gamma-ray emission above 100 TeV from 12 sources (Cao et al. 2021a; The LHAASO Collaboration et al. 2021; Cao et al. 2021b), which are probably the Galactic accelerators of PeV cosmic-rays, namely, PeVatrons. According to gamma-ray observations, various PeVatron candidates had been proposed, including, e.g., the Galactic center (e.g. HESS Collaboration et al. 2016), supernova remnants (SNRs, e.g. Tibet ASY Collaboration et al. 2021), pulsar wind nebulae (PWNe, e.g. Arons 2012) and young massive star clusters (YMCs, e.g. Aharonian et al. 2019).

However, the detection of gamma-rays up to multi-hundred TeV is not sufficient to identify the sources as cosmic-ray PeVatrons, because the gamma-rays can be produced by leptonic processes (i.e. inverse Compton scattering of electrons) as well. The detection of neutrinos, in company with the  $\pi^0$  decay gamma-rays, can definitely help to identify PeVatron sources.

Most of LHAASO sources have TeV counterparts. The high energy neutrinos from these TeV counterparts have been studied in the

previous works (e.g. Kappes et al. 2009; Halzen et al. 2017) and more sophisticated neutrino emission models have been proposed for some of them, including the Crab Nebula (e.g. Amato et al. 2003), Cygnus Region (e.g. Anchordoqui et al. 2007; Bykov et al. 2021) and SNR G106.3+2.7 (e.g. Ge et al. 2021).

IceCube, a km<sup>3</sup> neutrino detector at the South Pole, has searched for time-integrated neutrino emission from these TeV gamma-ray sources (e.g. Abbasi et al. 2011; Aartsen et al. 2013, 2017a, 2019, 2020). In a recent search, IceCube measured the astrophysical neutrinos from the direction of a list of neutrino source candidates with the ten-year data from 2008 to 2018 (Aartsen et al. 2020). MGRO J1908+06 is the most significant Galactic source in the search list but its local pre-trial p-value is only 0.038 which is far away from the  $3\sigma$  level. Only the upper limits on the neutrino flux from the point-like neutrino source candidates are provided under the assumptions of  $E^{-2}$  and  $E^{-3}$  neutrino spectra.

The upper limits on neutrino flux depend on the assumptions on the source extensions and spectral shapes. In this work, in order to evaluate the effect of these assumptions on the upper limit estimate, we use the Bayesian method and the ten-year IceCube muon-track data (IceCube Collaboration et al. 2021) from 2008 to 2018 to measure the neutrino flux from LHAASO sources and constrain the hadronic components of these gamma-ray sources. Our Bayesian method is based on the form of unbinned likelihood function which is widely used in the neutrino source searches (Braun et al. 2008; Abbasi et al. 2011; Aartsen et al. 2014, 2017b, 2019, 2020; Kochocki et al. 2021; Zhou et al. 2021). Several neutrino telescopes are under construction or planned, thus we further evaluate the detection of neutrinos from the LHAASO sources, assuming all the gamma-ray observed are produced by cosmic-rays, and estimate the observation time to obtain a  $5\sigma$  result. Multiple neutrino detectors are considered, including the detector in operation (e.g. IceCube and Baikal-GVD (Zaborov

★ E-mail: htq@pku.edu.cn

† E-mail: zhuo.li@pku.edu.cn

2020)), under construction (e.g. KM3NeT-ARCA (Adrián-Martínez et al. 2016)) and proposed (e.g. P-ONE (Agostini et al. 2020) and IceCube-Gen2 (Aartsen et al. 2021)).

This paper is organized as follows. In section 2, we introduce the IceCube muon-track data. In section 3, we describe the Bayesian method used for our analyses and the relationship between hadronic gamma-rays and neutrinos. In section 4, we compare the gamma-ray observations with the upper limits of hadronic gamma-ray flux and discuss the uncertainties in upper limit estimate. In section 5, we estimate the significance of signals in the combined search for neutrinos from LHAASO sources in the future. We finally summarize and discuss in section 6.

## 2 NEUTRINO DATA FROM ICECUBE

IceCube released the muon-track data from 2008 to 2018 which is used in the ten-year search (IceCube Collaboration et al. 2021). The data is composed of three parts: the experimental data events, the instrument response functions and the detector uptime.

The experimental data events are grouped into five samples including IC40, IC59, IC79, IC86-I and IC86-II, corresponding to different construction levels of the detector. The number in the sample name represents the number of strings in the detector. Digital Optical Modules on the string record the Cherenkov light from the charged particles produced in the neutrino-nucleus interactions ( $\nu + N$ ). The interaction time, the reconstructed direction and the reconstructed energy are given for each event. We should note that the reconstructed energy  $E_{\text{rec}}$  is the energy of muon ( $\nu_\mu + N \xrightarrow{\text{CC}} \mu + X$ ) passing through the detector, which is different from the energy of incident neutrino  $E_\nu$ .

The instrument response functions include the effective area and the smearing matrix. The effective area  $A_{\text{eff}}$  relies on the neutrino energy  $E_\nu$  and the declination angle  $\delta_\nu$ . The smearing matrix  $\mathcal{M}(E_{\text{rec}}|E_\nu, \delta_\nu)$  is the fractional count of simulated events in the reconstructed energy bin relative to all events in the  $(E_\nu, \delta_\nu)$  bin. The matrix tells us the probability to get the reconstructed energy  $E_{\text{rec}}$  when a neutrino with the energy  $E_\nu$  enters the detector from the declination  $\delta_\nu$ .

The detector uptime records the time periods during which the detector is running well. We can get the livetime of detector for each data sample.

## 3 BAYESIAN METHOD FOR SIGNAL SEARCH

We use the Bayesian method to search for signal events from the experimental data. The first step is to build the likelihood function. As for a source at the position  $\vec{x}_s = (\alpha_s, \delta_s)$  ( $\alpha_s$  is the right ascension and  $\delta_s$  is the declination angle), the likelihood ( $L$ ) for observing  $n_s$  signal events ( $dN_\nu/dE_\nu \propto E_\nu^{-\gamma}$ ) is given by the product of probability density functions (PDFs) for each track event

$$L = \prod_k \prod_i^{N_k} \left( \frac{n_s^k}{N_k} S_i + \frac{N_k - n_s^k}{N_k} B_i \right),$$

$$S_i = S^{\text{spat}}(\vec{x}_i, \sigma_i | \vec{x}_s) \times S^{\text{ener}}(E_i, \vec{x}_s | \gamma),$$

$$N_i = B^{\text{spat}}(\delta_i) \times B^{\text{ener}}(E_i, \delta_i),$$
(1)

where  $k, k' \in \{\text{IC40, IC59, IC79, IC86-I, IC86-II}\}$  represent five data samples. The expected number of signal events in data sample  $k$

( $n_s^k$ ) is proportional to the product of effective area  $A_{\text{eff}}^k$  and detector livetime  $t_k$ :

$$n_s^k = n_s \times \frac{\int t_k \int E_\nu^{-\gamma} A_{\text{eff}}^k(E_\nu, \delta_s) dE_\nu}{\sum_{k'} \int t_{k'} \int E_\nu^{-\gamma} A_{\text{eff}}^{k'}(E_\nu, \delta_s) dE_\nu}. \quad (2)$$

The spatial signal PDF  $S^{\text{spat}}$  describes the distribution of reconstructed directions  $\vec{x}_i$  for signal events from the source with an intrinsic extension  $\sigma_s$  and is assumed to follow a 2D Gaussian for each event with an individual angular uncertainty  $\sigma_i$ :

$$S^{\text{spat}} = \frac{1}{2\pi(\sigma_i^2 + \sigma_s^2)} \exp \left[ -\frac{|\vec{x}_i - \vec{x}_s|^2}{2(\sigma_i^2 + \sigma_s^2)} \right]. \quad (3)$$

The energy signal PDF  $S^{\text{ener}}$  describes the distribution of reconstructed energies  $E_i$  of signal events following an  $E_\nu^{-\gamma}$  neutrino spectrum from the direction of source  $\vec{x}_s$ . We use the effective area  $A_{\text{eff}}^k$  and the smearing matrix  $\mathcal{M}_k$  to build the energy signal PDF as

$$S^{\text{ener}} = \frac{\int E_\nu^{-\gamma} A_{\text{eff}}^k(E_\nu, \delta_s) dE_\nu \cdot \mathcal{M}_k(E_i | E_\nu, \delta_s)}{\int E_\nu^{-\gamma} A_{\text{eff}}^k(E_\nu, \delta_s) dE_\nu}. \quad (4)$$

The spatial background PDF  $B^{\text{spat}}$  and the energy background PDF  $B^{\text{ener}}$  are nearly uniform in right ascension. We assume that the background events follow the PDF of experimental data scrambled in right ascension. For each data sample, we count the number of events  $N_{ij}^k$  with declination  $\sin \delta \in [\sin \delta_i, \sin \delta_i + 0.02]$  and reconstructed energy  $\log_{10} E_{\text{rec}} \in [\log_{10} E_j, \log_{10} E_j + 0.1]$ . So the spatial background PDF and the energy background PDF are given as

$$B^{\text{spat}} = \frac{\sum_j N_{ij}^k}{N_k \times \Delta \Omega}, \quad B^{\text{ener}} = \frac{N_{ij}^k}{\sum_j N_{ij}^k}, \quad (5)$$

where  $N_k$  is the number of events in the data sample  $k$  and  $\Delta \Omega = 2\pi \Delta \sin \delta = 0.04\pi$ .

Figure 1 gives an example of the background and signal PDF. The left panel shows the spatial background PDF in five data samples. The right panel shows the energy PDF for background and signals in the direction of MGRO J1908+06.

As we have no preference on the signal event number, the prior distribution  $\pi(n_s)$  is assumed to be uniform in the range  $[0, N]$  for a known spectral index  $\gamma_0$  and a known source extension  $\sigma_0$ , where  $N = \sum_k N_k$  is the total number of events. The probability density of event number can be expressed as

$$p(n_s | X, \gamma_0, \sigma_0) = \frac{L(X | n_s, \gamma_0, \sigma_0) \pi(n_s)}{\int L(X | n_s, \gamma_0, \sigma_0) \pi(n_s) dn_s}, \quad (6)$$

where  $X$  represents the observed data. The cumulative probability  $\int^{n_{90}} p(n_s | \gamma_0, \sigma_0) dn_s = 0.9$  gives the 90% upper limit on signal event number  $n_{90}$ . The conversion between  $n_{90}$  and the 90% upper limit on neutrino flux  $\Phi_{\nu_\mu + \bar{\nu}_\mu}^{90\%} = dN/dE$  follows

$$n_{90} = \sum_k \int dt_k \int dE_\nu \Phi_{\nu_\mu + \bar{\nu}_\mu}^{90\%} A_{\text{eff}}^k(E_\nu, \delta_s). \quad (7)$$

Figure 2 shows an example of the cumulative probability function (CDF) for MGRO J1908+06 under the point source (PS) hypothesis and the extended source (ES) hypothesis. The extension of MGRO J1908+06 is around  $0.34^\circ$  (Aharonyan et al. 2009).

In hadronuclear ( $p\bar{p}$ ) scenarios, the neutrino flux and hadronic gamma-ray flux follows the relation as

$$\frac{1}{3} \sum_\alpha \frac{dN_{\nu_\alpha + \bar{\nu}_\alpha}}{dE_\nu} = K_\pi \frac{dN_\gamma}{dE_\gamma}, \quad (8)$$

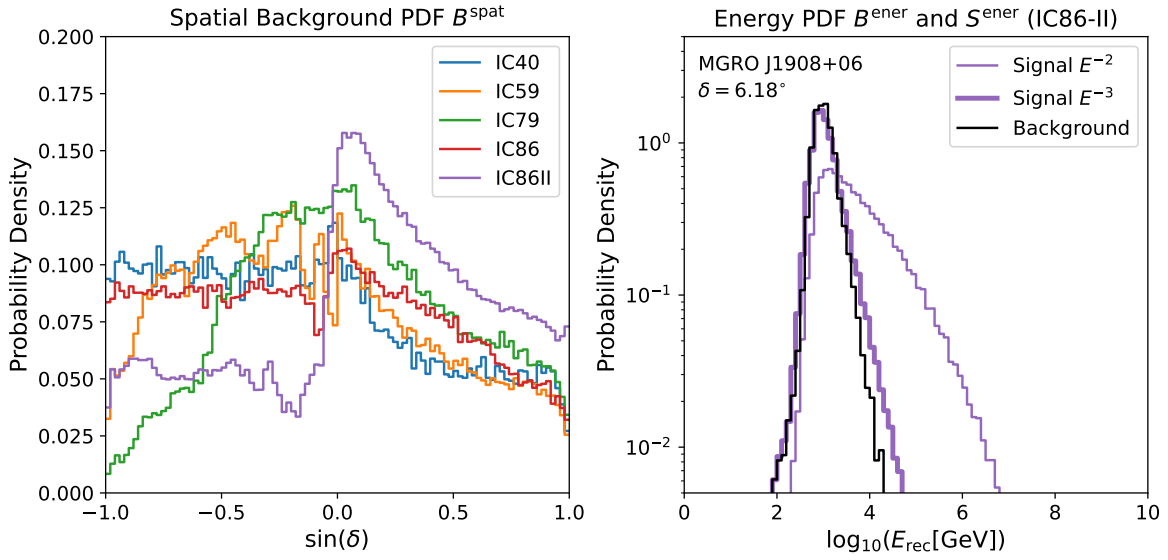


**Figure 1.** Left: the spatial background PDF. Different colors represent the PDFs for five data samples. Right: the energy background PDF and the energy signal PDF for MGRO J1908+06 (IC86-II). The thin (thick) purple line shows the energy signal PDF for an  $E^{-2}$  ( $E^{-3}$ ) neutrino spectrum. The black curve shows the energy background PDF at  $\delta_s = 6.18^\circ$ .

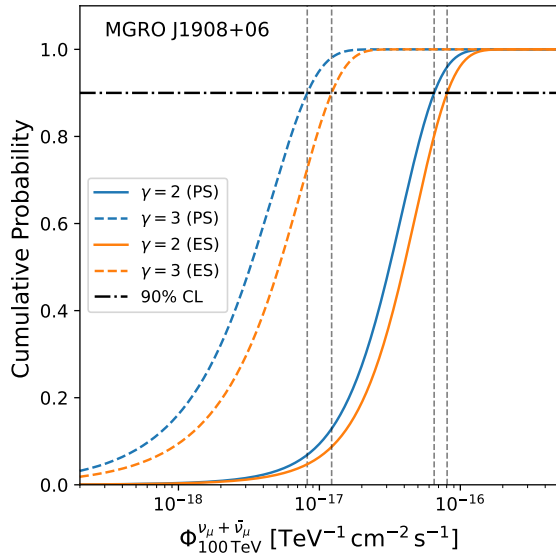


**Figure 2.** The cumulative probability of astrophysical neutrino flux at 100 TeV for MGRO J1908+06. Four different models are tested with two power-law indices  $\gamma = 2, 3$  and two neutrino source extensions  $\sigma_s = 0.0^\circ$  (PS),  $0.34^\circ$  (ES). The horizontal line indicates the 90% confidence level. The vertical lines indicate the 90% upper limit on astrophysical neutrino flux  $\Phi_{\nu_\mu + \bar{\nu}_\mu}^{90\%}$  for different models.

where  $\alpha = e, \mu, \tau$  represents the neutrino flavor,  $E_\gamma = 2E_\nu$ , and  $K_\pi \simeq 2$  is the number ratio of charged to neutral pions. Following this relation, we can transform the upper limit on neutrino flux into the upper limit on hadronic gamma-ray flux. The gamma-ray absorption ( $\gamma\gamma \rightarrow e^+e^-$ ) due to the interstellar radiation field (ISRF) and cosmic microwave background (CMB) is considered, if the distances to the TeV counterparts of LHAASO sources are available in the [TeVCat](#) (Wakely & Horan 2008). The ISRF energy density is taken from Popescu et al. (2017).

We should note that the spectrum term  $E_\nu^{-\gamma}$  in the likelihood function (see Equation 1) can be replaced by other spectral shapes (e.g., log-parabola model) or a specific neutrino emission model. So we can measure the astrophysical neutrino flux under any spectral shape assumptions.

#### 4 CURRENT RESULTS OF ICECUBE OBSERVATION

**Table 1** shows the parameters of intrinsic hadronic gamma-ray spectra before the  $\gamma\gamma$  absorption in propagation, which are tested in this work. Five models are considered:

$$\Phi_\gamma \propto \begin{cases} E_{10}^{-\gamma_1} & \text{(PL)} \\ E_{10}^{-\gamma_1 - \gamma_2 \log E_{10}} & \text{(LOGP)} \\ E_{10}^{-\gamma_1} \exp(-E/E_c) & \text{(ECPL)} \\ E_{10}^{-\gamma_1} \exp(-\sqrt{E/E_c}) & \text{(ECPL2)} \end{cases} \quad (9)$$

where  $E_{10} = E/10 \text{ TeV}$ , as well as the pulsar wind model proposed by Amato et al. (2003), where  $\mu$  is a dimensionless parameter describing the target density in the nebula,  $\Gamma$  is the wind Lorentz factor and  $f_p$  is the fraction of spin down luminosity carried by protons. The source extensions in **Table 1** are chosen according to the extension measurements of TeV counterparts and the prior extension of LHAASO sources (see details about the TeV counterparts in [Appendix A](#)).

In [Figure 3](#), we compare the 90% C.L. upper limits on hadronic gamma-ray flux (thick lines) with the observed gamma-ray flux (thin lines). Only the hadronic gamma-ray component of Crab Nebula is well constrained to be no more than 70% of total gamma-ray flux, which is consistent with the conclusion by Huang & Li (2021). More than 95% of neutrino signal events are expected below 25 TeV, corresponding to the hadronic gamma-ray energy below 50 TeV. The IceCube data mainly constrain the hadronic component below 50 TeV, rather than the new observations from 100 TeV to PeV given by LHAASO. The central energy ranges for LHAASO J1825-1326,

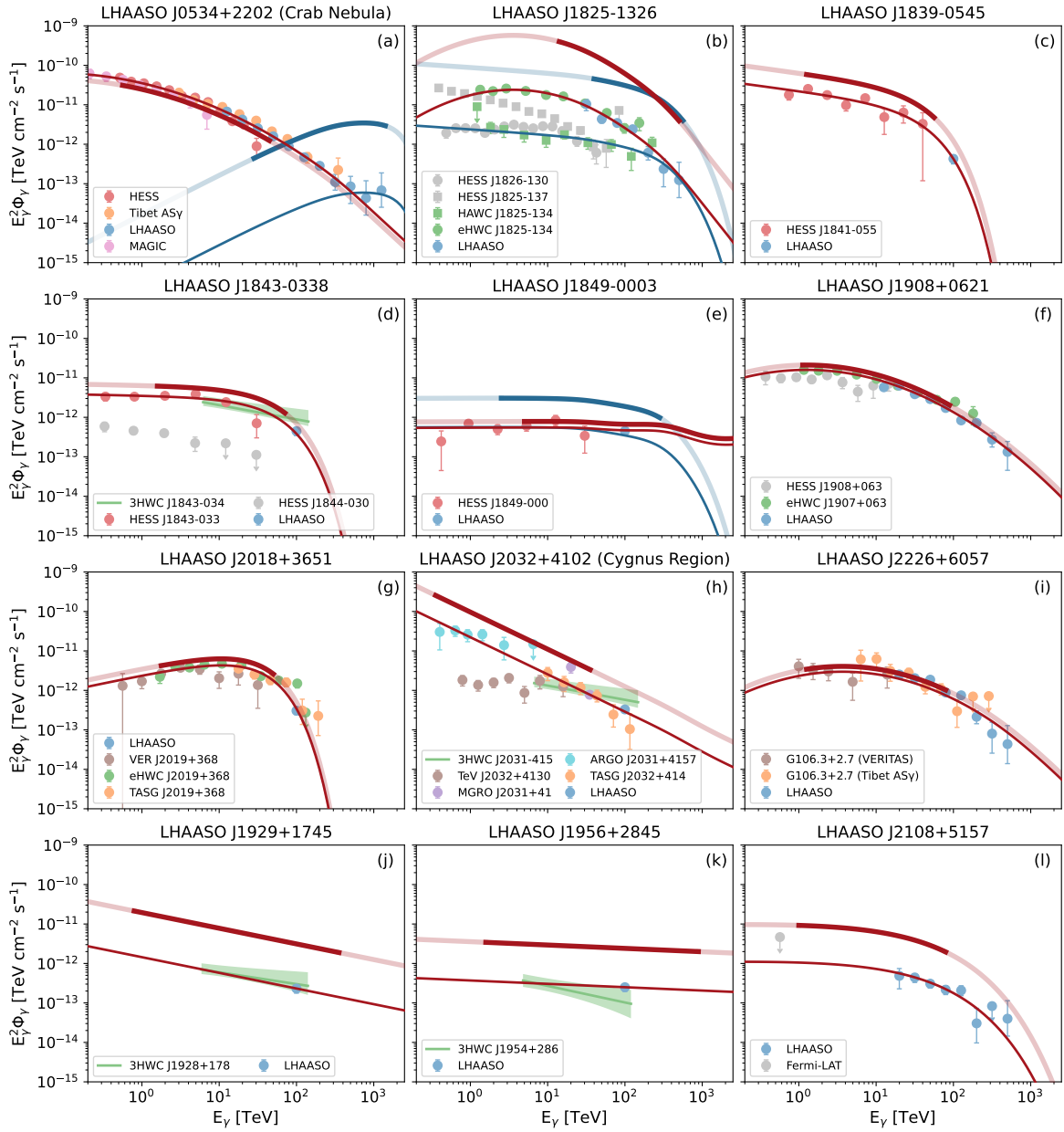


**Figure 3.** The 90% C.L. upper limits on hadronic gamma-ray flux (thick lines) from LHAASO sources and the observed gamma-ray flux (thin lines). The dark parts of thick lines mark the central 90% energy ranges according to neutrino observations. For each LHAASO source, the first model in Table 1 is shown as red, while the second model is shown as blue. Blue symbols are LHAASO observations (Cao et al. 2021a; The LHAASO Collaboration et al. 2021; Cao et al. 2021b). Other symbols and shaded areas are the gamma-ray measurements of (a) Crab Nebula by Tibet AS $\gamma$  (Amenomori et al. 2019), H.E.S.S. (Aharonian et al. 2006) and MAGIC (Albert et al. 2008); (b) HESS J1826-130 (H. E. S. S. Collaboration et al. 2020), HESS J1825-137 (H. E. S. S. Collaboration et al. 2019), eHWC J1825-134 (Abeysekara et al. 2020); (c) HESS J1841-055 (Aharonian et al. 2008); (d) HESS J1843-033 and HESS J1844-030 (H. E. S. S. Collaboration et al. 2018), 3HWC J1843-034 (Albert et al. 2020); (e) HESS J1849-000 (H. E. S. S. Collaboration et al. 2018); (f) HESS J1908+063 (Aharonian et al. 2009), eHWC J1907+063 (Abeysekara et al. 2020); (g) VER J2019+368 (Abeysekara et al. 2018), eHWC J2019+368 (Abeysekara et al. 2020), TAGS J2019+368 (Amenomori et al. 2021); (h) TeV J2032+4130 (Aliu et al. 2014), MGRO J2031+41 (Abdo et al. 2007, 2009), 3HWC J2031-415 (Albert et al. 2020), TAGS J2032+414 (Amenomori et al. 2021), ARGO J2031+4157 (Bartoli et al. 2014); (i) G106+2.7 by VERITAS (Acciari et al. 2009) and Tibet AS $\gamma$  (Tibet AS $\gamma$  Collaboration et al. 2021); (j) 3HWC J1928+178 (Albert et al. 2020); (k) 3HWC J1954+286 (Albert et al. 2020); (l) 4FGL J2108.0+5155 (Cao et al. 2021b). The gamma-ray absorption due to ISRF and CMB is considered if the distance is available.

HAWC J1825-134, LHAASO J1849-0003, LHAASO J1929+1745 and LHAASO J1956+2845 cover the multi-hundred TeV energies but their upper limits are higher than the gamma-ray fluxes observed.

Some factors leading to uncertainties in the analysis should be noted here. The assumptions on the extension of neutrino sources

affect the measurements of neutrinos/hadronic gamma-rays from LHAASO sources. Figure 4 shows the dependence of upper limits on source extensions. The extended-source hypothesis brings higher upper limits in comparison with the point-source hypothesis. If the extensions of Crab Nebula and LHAASO J1908+0621 are lower than

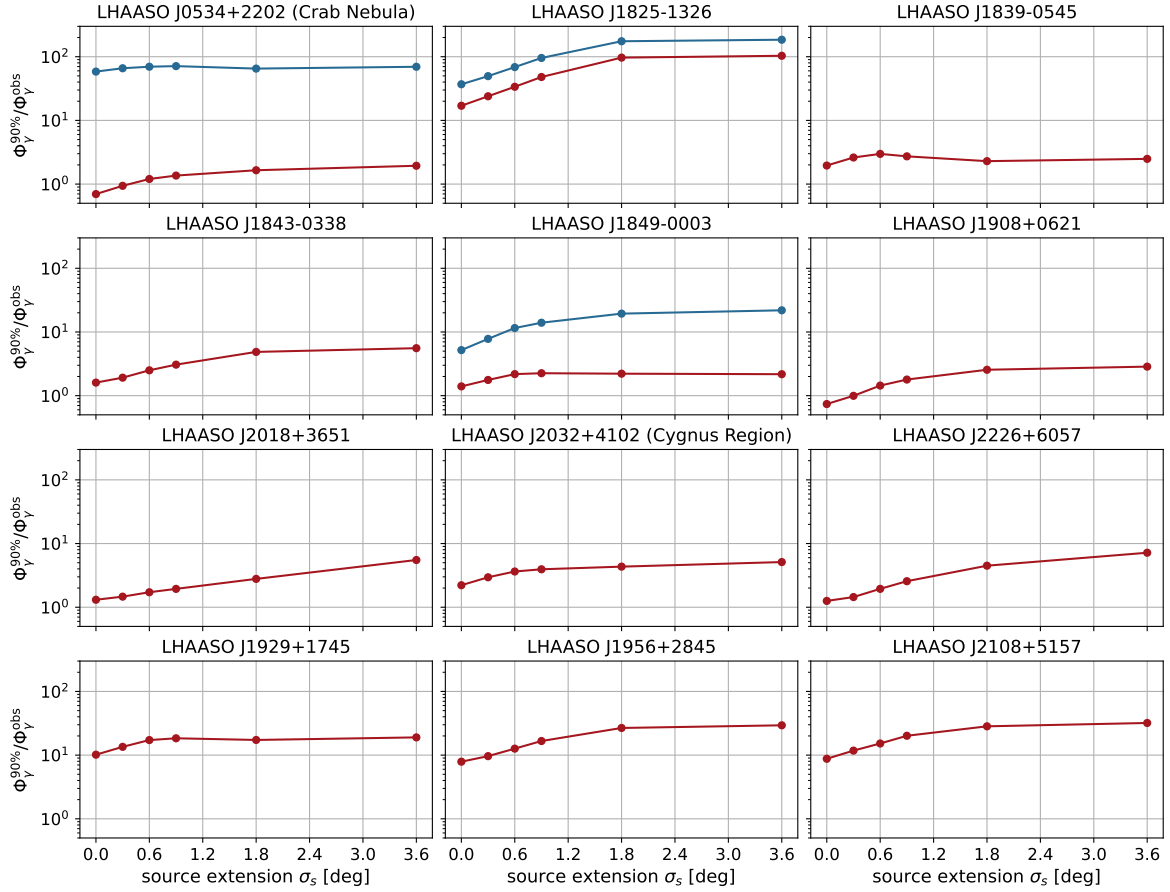


**Figure 4.** The flux ratio between the 90% hadronic gamma-ray flux  $\Phi_{\gamma}^{90\%}$  and the observed gamma-ray flux  $\Phi_{\gamma}^{\text{obs}}$  for different source extensions  $\sigma_s$ . The red (blue) lines correspond to the spectral shapes of hadronic gamma-rays following the red (blue) lines in Figure 3. These results are based on the ten-year IceCube data.

LHAASO Source	$\sigma_s$ [deg]	$\gamma_1$	$\gamma_2$	$E_c$ [TeV]	Model
J0534+2202	0.0	2.86	0.20	—	LOGP
J1825-1326	0.30	2.40	0.45	—	LOGP
	0.0	2.13	—	286	ECPL
J1839-0545	0.41	2.26	—	36	ECPL
J1843-0338	0.24	2.03	—	48	ECPL
J1849-0003	0.09	1.99	—	—	SPL
	0.09	1.99	—	300	ECPL
J1908+0621	0.52	2.53	0.30	—	LOGP
J2018+3651	0.20	1.57	—	26	ECPL
J2032+4102	1.8	2.94	—	—	SPL
J2226+6057	0.24	2.29	0.33	—	LOGP
J1929+1745	0.30	2.40	—	—	SPL
J1956+2845	0.30	2.09	—	—	SPL
J2108+5157	0.0	1.95	—	20	ECPL2
Source Name	$\sigma_s$ [deg]	$\mu$	$\Gamma$	$f_p$	Model
J0534+2202	0.0	1	$10^7$	0.15	Amato et al.

**Table 1.** The source extensions ( $\sigma_s$ ) and the parameters of hadronic gamma-ray spectra tested in this work. These spectra are also shown in Figure 3. The second spectrum is shown as blue line for each LHAASO source.

0.3°, the hadronic component of them can be constrained with the ten-year IceCube data.

The statistical method also affect the estimation on upper limits.

We choose 20 sources (including the seven sources associated with LHAASO sources) from the Table III of ten-year search by IceCube (Aartsen et al. 2020) and compare their upper limits<sup>1</sup> with the upper limits given by our Bayesian method. Our upper limits tend to be  $1.4^{+0.6}_{-0.2}$  ( $0.9^{+0.2}_{-0.3}$ ) times of the upper limits given by IceCube for the  $E^{-2}$  ( $E^{-3}$ ) neutrino spectrum.

The differences between the upper limits given by two methods are probably owing to multiple reasons: 1) The difference of statistical approaches. IceCube uses the Frequentist approach while we use the Bayesian approach. The results given by Bayesian approach relies on the uniform prior distribution  $\pi(n_s)$ . 2) The difference of the likelihood functions. The likelihood function of IceCube has two free parameters  $n_s$  and  $\gamma$ , while our likelihood function only has one free parameter  $n_s$ . 3) The difference of background PDF. The spatial background PDF  $B^{\text{spat}}$  and energy background PDF  $B^{\text{ener}}$  are precise parameterized with good data/Monte Carlo agreement Aartsen et al. (2016, 2019), while ours are obtained from the data.

Additionally, we also estimate the significance of signal neutrino events for different source extensions (see Appendix B for detailed calculation). We find that the three most significant sources are LHAASO J2032+4102 ( $\delta_s = 0.3^\circ$ ), LHAASO J1929+1745 ( $\delta_s = 0.6^\circ$ ) and LHAASO J1908+0621 (PS).

<sup>1</sup> The upper limits for  $E^{-2}$  ( $E^{-3}$ ) spectrum are taken from Table III (Figure 3) of Aartsen et al. (2020).

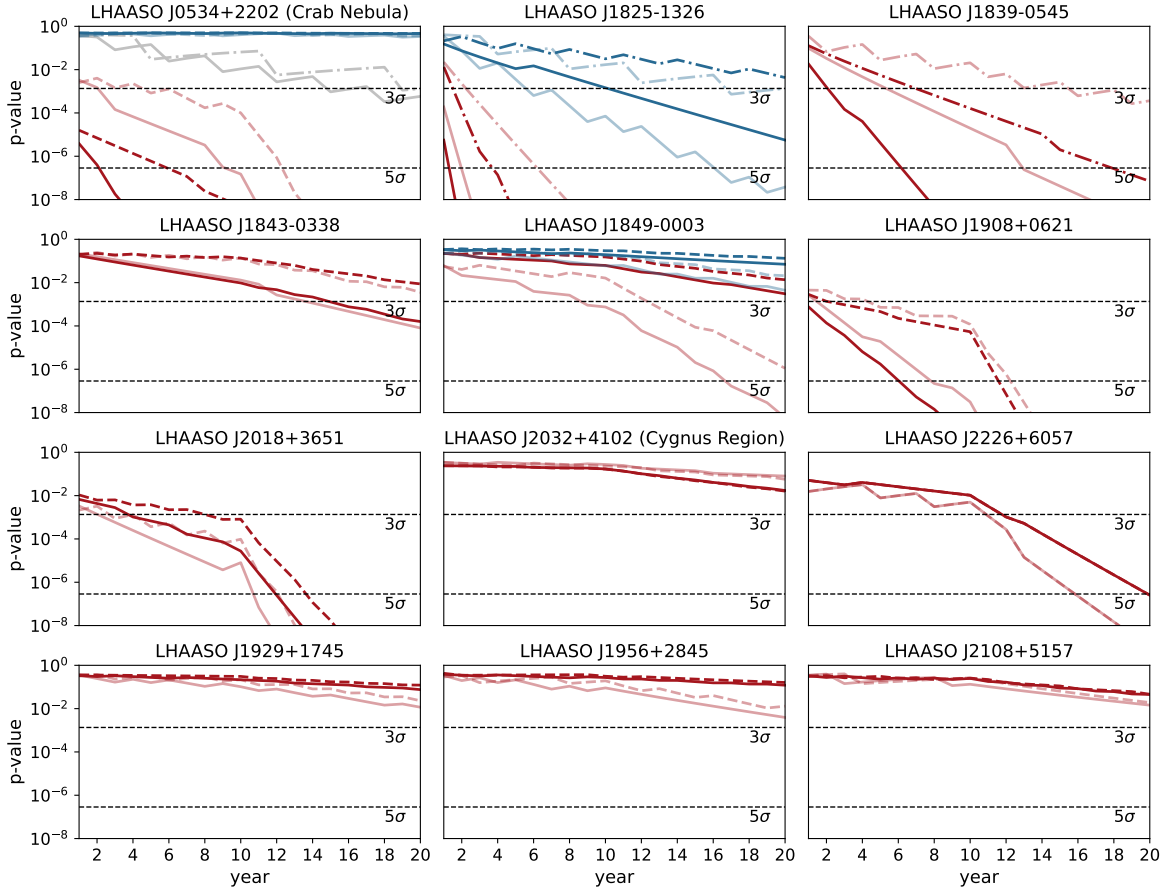


**Figure 5.** The p-values as a function of observation time. There are two groups of lines. Group I: The red (blue) lines correspond to the hadronic gamma-ray emission following the red (blue) thin lines in Figure 3; the solid lines: 10yr IceCube (2008-2018)+10yr PLE $\nu$ M-1+10yr PLE $\nu$ M-2; the dashed lines (source declination  $\delta_s > -5^\circ$ ): 10yr IceCube (2008-2018)+10yr IceCube+10yr IceCube-Gen2; the dash-dotted lines (source declination  $\delta_s < -5^\circ$ ): 20yr IceCube-like detector at the Lake Baikal; the dark lines: lower threshold energy  $E_{th} = 1$  TeV; the light lines: higher threshold energy  $E_{th} = 10$  TeV. Group II: The gray lines (only in the first panel) correspond to the pulsar wind model by Amato et al. (2003); the solid line: 20yr 30×IceCube-like detector at the South Pole; the dash-dotted line: 20yr 30×IceCube-like detector at the Lake Baikal; the threshold energy  $E_{th} = 100$  TeV.

## 5 PROSPECT OF FUTURE OBSERVATION

We evaluate the detection of neutrinos from LHAASO sources with the Planetary Neutrino Monitoring System (PLE $\nu$ M) which is a concept of global repository of high-energy neutrino observations made by current and future neutrino telescopes proposed by Schumacher et al. (2021). PLE $\nu$ M-1 consists of IceCube and IceCube-like detectors at the latitudes of Baikal-GVD, KM3NeT-ARCA and P-ONE, while PLE $\nu$ M-2 consists of IceCube-like detectors and IceCube-Gen2. We assume that the effective area of IceCube-Gen2 is around 7.5 times larger than IceCube.

We estimate the statistical significance of observation with the analytical expression of p-value ( $p_{value}$ ):

$$p_{value} = \frac{1}{2} \left[ 1 - \text{erf} \left( \sqrt{q_0^{obs}/2} \right) \right], \quad (10)$$

$$q_0^{obs} = 2 \left[ Y_b - N_D + N_D \ln \left( \frac{N_D}{Y_b} \right) \right],$$

where  $Y_b$  is the expected number of events for background hypothesis and  $N_D$  is the median of events Poisson-distributed around the signal plus background. We count the number of events within the opening angle  $\Omega = \pi\sigma_{\text{eff}}^2$  around the source, where the angle  $\sigma_{\text{eff}} = \sqrt{\sigma_s^2 + (1.6\Delta\xi_{\text{det}})^2}$ . The angular resolution  $\Delta\xi_{\text{det}}$  is around

$0.4^\circ$  for IceCube and  $0.2^\circ$  or better for the detectors in water like Baikal-GVD, KM3NeT and P-ONE. The opening angle  $\Omega$  contains roughly 72% of signal events from the source. This method has been applied to evaluate the prospects for detecting the neutrino emission from Galactic sources with IceCube (Halzen et al. 2017).

We count the event number of neutrinos above the threshold energy  $E_{th}$  within the opening angle  $\Omega$ . The background events for up-going track events are mainly induced by atmospheric muon neutrinos. The software MCEq (Fedynitch et al. 2015) is employed to model the background component of atmospheric neutrinos assuming the flux model Gaisser-H4a (Gaisser 2012) for primary cosmic rays and the hadronic interaction model Sibyll2.3c (Fedynitch et al. 2019). Only the up-going track events with the zenith angle  $\theta_z$  over  $85^\circ$  are considered here, because the discovery potential is several times to several orders of magnitude better in the northern sky for IceCube (see Figure 3 of Aartsen et al. 2020). The visibility ( $\theta_z > 85^\circ$ ) of each LHAASO source due to the Earth's spin is considered.

The red and blue lines in Figure 5 show the significance of observation if the hadronic gamma-rays follow the energy spectra (thin lines) in Figure 3. We use the data observed by PLE $\nu$ M-1 in the first ten years and by PLE $\nu$ M-2 in the next ten years in combination with the ten-year (2008-2018) data by IceCube. Within the twenty years, six LHAASO sources will be discovered at the

level of  $5\sigma$  for the threshold energy  $E_{\text{th}} = 1 \text{ TeV}$ , including Crab Nebula, LHAASO J1825-1326, LHAASO J1839-0545, LHAASO J1908+0621, LHAASO J2108+3651 and LHAASO J2226+6057. HAWC J1825-134 and LHAASO J1849-0003 (without cutoff) are also observable at the level of  $5\sigma$  for a higher threshold energy  $E_{\text{th}} = 10 \text{ TeV}$ .

In the neutrino source search by IceCube and IceCube-Gen2, Crab Nebula, LHAASO J1908+0621, LHAASO J2018+3651 and LHAASO J2226+6057 will be discovered within 20 years. The first three sources are consistent with the predictions in the Figure 18 of Aartsen et al. (2021). In the combined search, the help of IceCube-like detectors at the north hemisphere is significant in the observations of sources around the equatorial plane or at the southern sky ( $\delta_s < 5^\circ$ ). Even one IceCube-like detector at the latitude of Baikal-GVD will provide a  $5\sigma$  result around 4 years if the gamma-rays from LHAASO J1825-1326 are fully hadronic in origin.

In Figure 5, the blue lines for Crab Nebula overlap with each other and nearly don't evolve within the twenty years. If we want to observe these neutrinos at the level of  $3\sigma$  within 20 years, a very large neutrino detector is required, whose effective area is 30 times larger than IceCube (see gray lines in Figure 5).

## 6 SUMMARY AND DISCUSSION

We analyze the ten-year IceCube data with Bayesian approach to measure the hadronic gamma-ray flux from the direction of LHAASO sources and give the 90% C.L. upper limit for extended-source and point-source hypotheses. The results given by the Bayesian approach rely on the uniform prior distribution. We further evaluate the combined search for high energy neutrinos from LHAASO sources with IceCube, IceCube-Gen2 and IceCube-like detectors at the latitude of Baikal-GVD, KM3NeT-ARCA, P-ONE.

The main conclusions are summarized as: **i**) The 90% C.L. upper limit on hadronic gamma-ray flux from Crab Nebula is around 70% of total gamma-ray flux observed; **ii**) Seven LHAASO sources and HAWC J1825-134 are expected to be discovered at the level of  $5\sigma$  by PLEvM-1 and PLEvM-2 within 20 years, if their gamma-rays are fully hadronic in origin; **iii**) An IceCube-like detector at the location of Baikal-GVD is expected to give a  $5\sigma$  result around 4 years if all the gamma-rays from LHAASO J1825-1326 are hadronic in origin.

In our analysis, the three most significant sources are LHAASO J2032+4102, LHAASO J1929+1745 and LHAASO J1908+0621. Under the point-source hypothesis, the pre-trial p-value is 0.056 for LHAASO J1908+0621 and 0.092 for LHAASO J2032+4102 which are similar with the p-values in the directions of MGRO J1908+06 and 2HWC J2031+415 in the ten-year search by IceCube (Aartsen et al. 2020). The TeV counterparts of LHAASO J1929+1745 are not in the source list of ten-year search because they are not that luminous in the TeVCat (Wakely & Horan 2008). LHAASO J1929+1745 is even one of the dimmest LHAASO sources at 100 TeV energy (Cao et al. 2021a). Mori et al. (2020) have tried to explain the gamma-rays from 2HWC J1928+177 ( $0.10^\circ$  from LHAASO J1929+1745) with a hadronic accelerator model.

The neutrino constraint on Crab Nebula disfavors hadronic process dominates the bulk of the observed gamma-ray emission, while the gamma-ray spectrum has a possible hardening around PeV energies. If the PeV gamma-rays are hadronic in origin, a neutrino detector with the effective area  $\sim 30$  times larger than IceCube is required to observe the neutrinos associated with these PeV gamma-rays at the level of  $3\sigma$  within 20 years (see the first panel in Figure 5).

The Baikal-GVD has deployed 8 clusters and plans to add two

clusters every year from 2022 to 2024, occupying a water volume around  $0.7 \text{ km}^3$  in total (Baikal-GVD Collaboration et al. 2021). A KM3NeT-ARCA block comprises 115 strings and eleven detection units has been deployed (KM3NeT Collaboration et al. 2021). P-ONE has deployed two pathfinders and the design of the P-ONE neutrino telescope is underway (Bailly et al. 2021). The P-ONE Explorer (10 strings) is planned to deploy in 2023-2024 and remainder of the array (70 strings) is planned for deployment between 2028-2030 (Agostini et al. 2020). IceCube-Gen2 is planned for deployment between 2027-2033. PLEvM-1 wil start to operate after 2030, while PLEvM-2 wil start to operate after 2033. These neutrino source candidates are expected to be identified or excluded at the high confidence level from 2030 to 2050.

## ACKNOWLEDGMENTS

We thank Hao Zhou and Xiao-Yuan Huang for useful discussions. This work is supported by the Natural Science Foundation of China (No. 11773003, U1931201) and the China Manned Space Project (CMS-CSST-2021-B11). This research has made use the TeVCat online source catalog (<http://tevcat.uchicago.edu>).

## REFERENCES

Aartsen M. G., et al., 2013, *ApJ*, **779**, 132  
 Aartsen M. G., et al., 2014, *ApJ*, **796**, 109  
 Aartsen M. G., et al., 2016, *ApJ*, **833**, 3  
 Aartsen M. G., et al., 2017a, *ApJ*, **835**, 151  
 Aartsen M. G., et al., 2017b, *ApJ*, **849**, 67  
 Aartsen M. G., et al., 2019, *European Physical Journal C*, **79**, 234  
 Aartsen M. G., et al., 2020, *Phys. Rev. Lett.*, **124**, 051103  
 Aartsen M. G., et al., 2021, *Journal of Physics G Nuclear Physics*, **48**, 060501  
 Abbasi R., et al., 2011, *ApJ*, **732**, 18  
 Abdo A. A., et al., 2007, *ApJ*, **664**, L91  
 Abdo A. A., et al., 2009, *ApJ*, **700**, L127  
 Abeysekara A. U., et al., 2018, *ApJ*, **861**, 134  
 Abeysekara A. U., et al., 2020, *Phys. Rev. Lett.*, **124**, 021102  
 Acciari V. A., et al., 2009, *ApJ*, **703**, L6  
 Adrián-Martínez S., et al., 2016, *Journal of Physics G Nuclear Physics*, **43**, 084001  
 Agostini M., et al., 2020, *Nature Astronomy*, **4**, 913  
 Aharonian F., et al., 2006, *A&A*, **457**, 899  
 Aharonian F., et al., 2008, *A&A*, **477**, 353  
 Aharonian F., et al., 2009, *A&A*, **499**, 723  
 Aharonian F., Yang R., de Oña Wilhelmi E., 2019, *Nature Astronomy*, **3**, 561  
 Albert J., et al., 2008, *ApJ*, **674**, 1037  
 Albert A., et al., 2020, *ApJ*, **905**, 76  
 Albert A., et al., 2021, *ApJ*, **907**, L30  
 Aliu E., et al., 2014, *ApJ*, **783**, 16  
 Amato E., Guetta D., Blasi P., 2003, *A&A*, **402**, 827  
 Amenomori M., et al., 2019, *Phys. Rev. Lett.*, **123**, 051101  
 Amenomori M., et al., 2021, *Phys. Rev. Lett.*, **127**, 031102  
 Anchordoqui L. A., Beacom J. F., Goldberg H., Palomares-Ruiz S., Weiler T. J., 2007, *Phys. Rev. D*, **75**, 063001  
 Arons J., 2012, *Space Sci. Rev.*, **173**, 341  
 Baikal-GVD Collaboration et al., 2021, arXiv e-prints, [p. arXiv:2106.06288](https://arxiv.org/abs/2106.06288)  
 Bailly N., et al., 2021, *European Physical Journal C*, **81**, 1071  
 Bartoli B., et al., 2014, *ApJ*, **790**, 152  
 Braun J., Dumm J., De Palma F., Finley C., Karle A., Montaruli T., 2008, *Astroparticle Physics*, **29**, 299  
 Bykov A. M., Petrov A. E., Kalyashova M. E., Troitsky S. V., 2021, *ApJ*, **921**, L10  
 Cao Z., et al., 2021a, *Nature*, **594**, 33  
 Cao Z., et al., 2021b, *ApJ*, **919**, L22

Cowan G., Cranmer K., Gross E., Vitells O., 2011, *European Physical Journal C*, **71**, 1554

Fedynitch A., Engel R., Gaisser T. K., Riehn F., Stanev T., 2015, in 34th International Cosmic Ray Conference (ICRC2015). p. 1129

Fedynitch A., Riehn F., Engel R., Gaisser T. K., Stanev T., 2019, *Phys. Rev. D*, **100**, 103018

Fesen R. A., Shull J. M., Hurford A. P., 1997, *AJ*, **113**, 354

Gaisser T. K., 2012, *Astroparticle Physics*, **35**, 801

Ge C., Liu R.-Y., Niu S., Chen Y., Wang X.-Y., 2021, *The Innovation*, **2**, 100118

H. E. S. S. Collaboration 2020, *Nature Astronomy*, **4**, 167

H. E. S. S. Collaboration et al., 2018, *A&A*, **612**, A1

H. E. S. S. Collaboration et al., 2019, *A&A*, **621**, A116

H. E. S. S. Collaboration et al., 2020, *A&A*, **644**, A112

HESS Collaboration et al., 2016, *Nature*, **531**, 476

Halzen F., Kheirandish A., Niro V., 2017, *Astroparticle Physics*, **86**, 46

Huang T.-Q., Li Z., 2021, arXiv e-prints, p. arXiv:2105.09851

IceCube Collaboration et al., 2021, arXiv e-prints, p. arXiv:2101.09836

KM3NeT Collaboration et al. 2021, Liveblog about the ongoing sea operation for ARCA, <https://www.km3net.org/blog-about-the-ongoing-sea-operation-for-arca/>

Kappes A., Halzen F., Murchadha A. Ó., 2009, *Nuclear Instruments and Methods in Physics Research A*, **602**, 117

Kochacki A., Takhistov V., Kusenko A., Whitehorn N., 2021, *ApJ*, **914**, 91

Mori K., et al., 2020, *ApJ*, **897**, 129

Popescu C. C., Yang R., Tuffs R. J., Natale G., Rushton M., Aharonian F., 2017, *MNRAS*, **470**, 2539

Schumacher L. J., Huber M., Agostini M., Bustamante M., Oikonomou F., Resconi E., 2021, arXiv e-prints, p. arXiv:2107.13534

The LHAASO Collaboration et al., 2021, *Science*, **373**, 425

Tibet ASY Collaboration et al., 2021, *Nature Astronomy*, **5**, 460

Wakely S. P., Horan D., 2008, International Cosmic Ray Conference, **3**, 1341

Wald A., 1943, *Transactions of the American Mathematical Society*, **54**, 426

Zaborov D., 2020, arXiv e-prints, p. arXiv:2011.09209

Zhou B., Kamionkowski M., Liang Y.-f., 2021, *Phys. Rev. D*, **103**, 123018

## APPENDIX A: TEV GAMMA-RAY COUNTERPARTS

In this appendix, we describe in some details about the TeV counterparts of LHAASO sources. Table A1 gives the distances and the extensions of these TeV counterparts.

**Crab Nebula.** LHAASO-KM2A has detected an 1.1 PeV photon from the direction of Crab Nebula and its energy spectrum has a possible hardening around PeV energies which indicates a hadronic component (The LHAASO Collaboration et al. 2021). So we consider the model by (Amato et al. 2003), in which protons takes  $f_p = 60\%$  of pulsar wind energy and produce gamma-rays and neutrinos through  $pp$  interactions. The target density  $n_t$  is expressed as

$$n_t = 10\mu(M_{N\odot}/R_{\text{pc}}^3) \text{ cm}^{-3} \quad (\text{A1})$$

with the parameter  $\mu$  defined in the Equation 9 of Amato et al. (2003). The  $pp$  interactions are dominant in comparison with the photo-meson ( $p\gamma$ ) productions if  $\mu$  is not very much smaller than unity. As for the target density  $\mu = 1$ , the gamma-ray flux will be higher than the observed flux if  $f_p > 15\%$ , while the peak energy won't be high enough if the wind Lorentz factor  $\Gamma < 10^7$ . The density parameter  $\mu$  equals to 5 if the mass estimated by Fesen et al. (1997) uniformly distributes in the nebula (Amato et al. 2003). The higher target density requires lower  $f_p$  to account for the observation.

**LHAASO J1825-1326.** HAWC has resolved region around eHWC J1825-134 into three sources (HAWC J1825-138, HAWC J1826-128 and HAWC J1825-134) and discovered the point-like source HAWC J1825-134 whose energy spectrum extends well beyond 200 TeV without a cutoff (Albert et al. 2021). As the angular distance between

HAWC J1825-134 and LHAASO J1825-1326 is only  $0.03^\circ$  (see Table A1), we fit the energy spectrum of HAWC J1825-134 in combination of the measurements by HAWC and LHAASO. The extrapolated flux ( $> 100$  TeV) of HAWC J1825-138 and HAWC J1826-128 are removed from the measurements by LHAASO.

**LHAASO J2032+4102.** The angular distances between LHAASO J2032+4102 and its TeV counterparts are larger than the angular resolution of LHAASO-KM2A around 15-20 arcmin at 100 TeV (Cao et al. 2021a). Such angular distances indicate that hundred TeV gamma-rays and TeV gamma-rays are probably generated in different emission regions or astrophysical sources. Further studies on the morphology and spectrum of this region are required to reveal the origin of PeV gamma-rays from Cygnus region.

**LHAASO J2108+5157.** LHAASO J2108+5157 is the only LHAASO source without TeV counterparts. As the constraint on TeV gamma-ray flux is not that strong, we refer the hadronic model shown in Figure 5 of Cao et al. (2021b) and use the ECPL2 in Equation 9 to model the profile of hadronic gamma-ray spectrum.

**Rescaling due to extension.** In Figure 3, the flux measurements of HESS J1826-130, HESS J1841-055, HESS J1908+063, VER J2019+368, TeV J2032+4130 and G106.3+2.7 (VERITAS) are rescaled according to their intrinsic extensions and integration regions. See details in Appendix B of Huang & Li (2021).

## APPENDIX B: SIGNAL SIGNIFICANCE FOR DIFFERENT SOURCE EXTENSIONS

In addition to the upper limits shown in Figure 3 and Figure 4, we give the significance of signal neutrino events from the direction of LHAASO sources in this section. A test statistic ( $TS$ ) is built as

$$TS = 2\ln \left[ \frac{L(X|\hat{n}_s, \sigma_0, \Phi_0^{\text{model}})}{L(X|\hat{n}_s = 0, \sigma_0, \Phi_0^{\text{model}})} \right], \quad (\text{B1})$$

where  $L$  is the likelihood function in Equation 1,  $X$  represents the observed data and  $\hat{n}_s$  is the number of signal events ( $n_s \geq 0$ ) maximizing the likelihood with given source extension  $\sigma_0$  and spectral shape  $\Phi_0^{\text{model}}$  (e.g.  $E^{-\gamma_0}$ ) of incident astrophysical neutrinos. Assuming the validity of the Wald approximation (Wald 1943),  $TS$  will follow the PDF as

$$f(TS) = \frac{1}{2} \delta(TS) + \frac{1}{2} \frac{1}{\sqrt{2\pi}} \frac{1}{\sqrt{TS}} e^{-TS/2} \quad (\text{B2})$$

for pure background hypothesis (Cowan et al. 2011). So the statistical significance of signal neutrino events can be described with the pre-trial p-value as  $1 - F(TS)$ , where  $F(TS)$  is the CDF of  $f(TS)$ :

$$F(TS) = \frac{1}{2} \left[ 1 + \text{erf} \left( \sqrt{TS/2} \right) \right]. \quad (\text{B3})$$

The p-values for different source extensions are shown in Figure B1.

This paper has been typeset from a  $\text{\TeX}/\text{\LaTeX}$  file prepared by the author.

LHAASO source	Extension [deg]	TeV Counterpart	Distance [kpc]	Angular Distance [deg]	Extension [deg]	Reference
J0534+2202	<b>PS</b>	Crab Nebula	2.0	0.08	0.01	[1]
J1825-1326	<b>0.30</b>	HESS J1826-130	4.0	0.39	0.21	[2]
		HESS J1825-137	3.9	0.39	0.55 (0.51)	[3]
		eHWC J1825-134	—	0.09	0.36	[4]
		HAWC J1825-134	—	0.03	<b>PS</b>	[5]
J1839-0545	ES	HESS J1841-055	—	0.29	<b>0.41</b>	[6]
J1843-0338	ES	HESS J1843-033	—	0.22	<b>0.24</b>	[6]
		HESS J1844-030	—	0.69	PS	[6]
		3HWC J1843-034	—	0.30	PS	[7]
J1849-0003	ES	HESS J1849-000	7	0.11	<b>0.09</b>	[6]
J1908+0621	0.58	HESS J1908+063	—	0.11	0.34	[8]
		eHWC J1907+063	—	0.14	<b>0.52</b>	[4]
J2018+3651	ES	VER J2019+368	—	0.10	0.34 (0.14)	[9]
		eHWC J2019+368	—	0.17	<b>0.20</b>	[4]
		TASG J2019+368	—	0.19	0.28	[10]
J2032+4102	ES	3HWC J2031+415	—	0.47	PS	[7]
		TeV J2032+4130	1.8	0.52	0.16 (0.07)	[11]
		ARGO J2031+4157	1.4	1.5	<b>1.8</b>	[12]
		TASG J2032+414	—	0.41	PS	[13]
		MGRO J2031+41	—	0.51	3.0	[14]
J2226+6057	0.36	G106.3+2.7 (VERITAS)	0.8	0.14	0.27 (0.18)	[15]
		G106.3+2.7 (Tibet AS $\gamma$ )	0.8	0.11	<b>0.24</b>	[16]
J1929+1745	ES	3HWC J1928+178	—	0.16	PS	[7]
J1956+2845	ES	3HWC J1954+286	—	0.33	PS	[7]
J2108+5157	PS	—	—	—	—	—

**Table A1.** The TeV counterparts associated with the LHAASO sources. The second column is the intrinsic extension of LHAASO sources. PS represents the point-like source while ES represents extended source. The prior intrinsic extension for extended LHAASO source is 0.3° (Cao et al. 2021a). The sixth column is the intrinsic extension of TeV counterparts. The number inside (outside) the brackets is the extension along the minor (major) axis. The extension in **bold** indicates the source extension adopted in Table 1. The distance from the TeV counterpart to us is taken from TeVCat (Wakely & Horan 2008). The extensions of TeV counterparts and their angular distances to the LHAASO source refer to [1] H. E. S. S. Collaboration (2020), [2] H. E. S. S. Collaboration et al. (2020), [3] H. E. S. S. Collaboration et al. (2019), [4] Abeysekara et al. (2020), [5] Albert et al. (2021), [6] H. E. S. S. Collaboration et al. (2018), [7] Albert et al. (2020), [8] Aharonian et al. (2009), [9] Abeysekara et al. (2018), [10] Amenomori et al. (2021), [11] Aliu et al. (2014), [12] Bartoli et al. (2014), [13] Amenomori et al. (2021), [14] Abdo et al. (2007), [15] Acciari et al. (2009) and [16] Tibet AS $\gamma$  Collaboration et al. (2021).

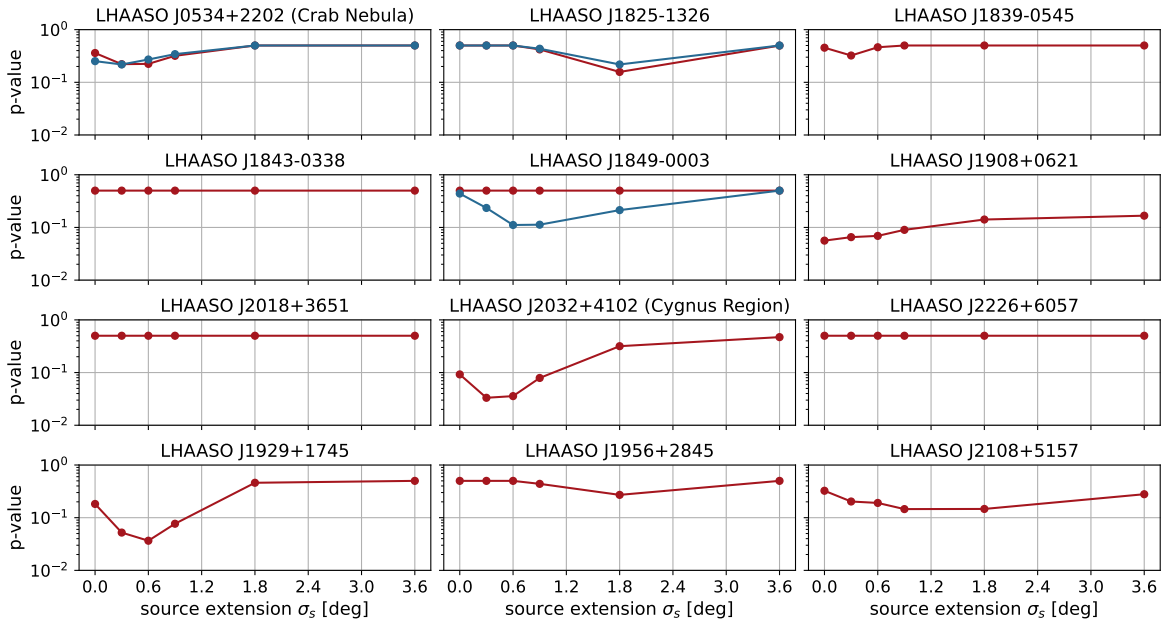


**Figure B1.** The statistical significance (p-values) of astrophysical neutrinos from LHAASO sources for different source extensions  $\sigma_s$ . The red (blue) lines correspond to the spectral shapes of hadronic gamma-rays following the red (blue) lines in Figure 3. These results are based on the ten-year IceCube data.